Photolysis of Nitrous Oxide Isotopomers Studied by Time-Dependent Hermite Propagation

Matthew S. Johnson,*,† Gert Due Billing,† Alytis Gruodis,‡ and Maurice H. M. Janssen§

Department of Chemistry, University of Copenhagen, Universitetsparken 5, DK-2100 Copenhagen Ø, Denmark, Department of General Physics and Spectroscopy, University of Vilnius, Sauletekio 9, b. 3, 2040 Vilnius, Lithuania, and Laser Centre and Department of Chemistry, Vrije Universiteit, De Boelelaan 1083, 1081 HV Amsterdam, The Netherlands

Received: April 18, 2001; In Final Form: June 25, 2001

Nitrous oxide (N_2O) plays an important role in greenhouse warming and ozone depletion. Yung and Miller's zero point energy (ZPE) model for the photolysis of N_2O isotopomers was able to explain atmospheric isotopomer distributions without invoking in situ chemical sources. Subsequent experiments showed enrichment factors twice those predicted by the ZPE model. In this article we calculate the UV spectrum of the key N_2O isotopomers to quantify the influence of factors not included in the ZPE model, namely, the transition dipole surface, bending vibrational excitation, dynamics on the excited state potential surface, and factors related to isotopic substitution itself. The relative cross-sections are calculated as the Fourier transform of the correlation function of the initial vibrational wave function and the time-propagated wave function, using a Hermite expansion of the time evolution operator. The model uses the electronic structure data recently published by Balint-Kurti and co-workers and makes several predictions. (a) The absolute values of the enrichment factors decrease with increasing temperature. (b) Photolysis of N_2O will produce "mass-independent" enrichment in the remaining sample. (c) Much of the enrichment is due to decreased heavy isotopomer cross-section over the entire absorption band, in contrast to the wavelength shift predicted by the ZPE model. Consequently, to within the error of the calculation, we predict only minor enrichments at $\lambda < 182$ nm. The smaller bending excursion of heavy isotopomers combines with the transition dipole surface to produce a smaller integrated cross-section. This effect is partially countered by the larger fraction of heavy isotopomers in excited bending states; the first three bending states have an integrated intensity ratio of ca. 1:3:6. The model agrees with available experimental enrichment factors and stratospheric balloon infrared remote sensing data to within the estimated error.

Introduction

Nitrous oxide (N_2O) is the second most abundant nitrogen species in the atmosphere, produced mainly by nitrifying and denitrifying bacteria in the soil and ocean. The preindustrial mixing ratio, measured in gas bubbles trapped in glacial ice, was 276 ppbv.[1] It is anticipated that the present-day mixing ratio of 316 ppbv will increase to ca. 400 ppbv by the end of the century. A third of the N_2O source is influenced by human activity, primarily nitrogen fertilizer, biomass burning, and animal husbandry, with minor contributions from nylon production and motor vehicle emissions.[2] N_2O is a greenhouse gas[3] with a per-molecule global warming potential 200−300 times that of CO_2; accordingly the Kyoto treaty addresses N_2O emissions. Unfortunately there are uncertainties of about 50% in source and sink fluxes, making regulation difficult.[2] Isotopic analysis has been used to understand and/or improve the budgets of atmospheric gases such as O_3, CH_4, CO_2, and CO.[4] Isotopic distributions in the main N_2O sources have been characterized;[5] in this paper we will consider the main sink reaction.

The atmosphere attenuates incoming radiation. A gap between the Shumann−Runge bands of molecular oxygen and the Hartley band of ozone (and the Herzberg continuum of O_2) allows energetic solar radiation to reach the lower stratosphere. At 20 km, the "UV window" extends from 197 to 214 nm.[6,7] The UV solar radiation photolyses several gases central to stratospheric chemistry, e.g., CFCs, OCS[8], and N_2O:

$$[1] \qquad N_2O + h\nu \rightarrow N_2 + O(^1D)$$

Reaction 1 (unit quantum yield, $D_0 = 351$ kJ/mol)[9] removes about 90% of atmospheric N_2O. The remaining sink is reaction with electronically excited oxygen atoms:

$$[2a] \qquad N_2O + O(^1D) \rightarrow 2NO \qquad (6\%)$$

$$[2b] \qquad N_2O + O(^1D) \rightarrow N_2 + O_2 \qquad (4\%)^{10}$$

Reactions [1] and [2] lead to an instantaneous lifetime of 123 years.[7] Reaction [2a] is the dominant source of reactive odd nitrogen to the stratosphere.[11] The odd nitrogen reaction cycle is now known to be the most important process removing nonpolar ozone.[12]

It is instructive to review the UV spectroscopy, electronic structure, and photodissociation dynamics of N_2O in order to understand isotope effects in reaction 1. Several authors have described the increase in absorption cross-section with temperature, especially on the red side of the absorption maximum.[13] The JPL advisory panel[6] recommends the parametrization given by Selwyn et al. for use in stratospheric modeling.[13a] The absorption feature is a peak centered at 182 nm, composed of a smooth-continuum absorption with weak vibronic structure to high energies, suggesting a repulsive or predissociative upper state. The absorption is dominated by the parallel transition $2\,^1A'(^1\Delta) \leftarrow X\,1^1A'(^1\Sigma^+)$, with additional involvement of the perpendicular transition $1\,^1A''(^1\Sigma^-) \leftarrow X\,1^1A'(^1\Sigma^+)$ (the symmetry species of the bent (linear) moiety is indicated).[14] While the $^1\Delta \leftarrow {}^1\Sigma^+$ transition is electronic-dipole-forbidden, the transition becomes allowed as the molecule bends. Using molecular orbital

* To whom correspondence should be addressed. Phone: +45 3532 0303. Fax: +45 3535 0609. E-mail: msj@kiku.dk.
† University of Copenhagen.
‡ University of Vilnius.
§ Vrije Universiteit.

10.1021/jp011449x CCC: $20.00
Published on Web 09/05/2001

notation, the parallel transition is $2\pi^3 3\pi \leftarrow 2\pi^4$; the 3π orbital is in the plane of the bend for the $2^1A'(^1\Delta)$ state.[15] Normal coordinate analysis of the vibronic structure indicates an upper-state bond angle of 115°,[16] indicating that a bent ground-state geometry will lead to a larger Franck−Condon overlap. Thus the temperature dependence may arise from participation by bending hot bands through vibronic interaction and the Franck−Condon factors. Selwyn and Johnston recorded the UV spectrum of several individual N_2O isotopomers; unfortunately, their original data is no longer available.[16]

Hopper mapped the electronic structure of N_2O in the early 1980s at the MCSCF/CI level.[14] For the linear $C_{\infty v}$ geometry there are two low-lying electronic states, $^1\Sigma^-$ and $^1\Delta$. The $^1\Delta$ state splits into the $2^1A'$ and $2^1A''$ Renner−Teller components upon bending (C_s), while the $^1\Sigma^-$ state becomes $1^1A''$. The $2^1A'$-($^1\Delta$) and $1^1A''(^1\Sigma^-)$ states are similar topologically, and the $2^1A''(^1\Delta)$ state increases in energy upon bending. Hopper found evidence for a bent excited-state geometry with bond angle of ca. 130°. More recently Janssen and co-workers performed CASSCF calculations to understand the photodissociation dynamics of the system.[17] Recently, Balint-Kurti and co-workers published the results of CASSCF calculations on the $^1A'$, $2^1A'$, and $1^1A''$ potential energy surfaces, along with transition dipole moment surfaces.[18]

While the UV photodissociation of N_2O is used as a clean source of $O(^1D)$ for kinetics studies, molecular beam studies show that the process is not simple. About 60% of the available energy is present within the $N_2(^1\Sigma^+)$ fragment, the remainder being translational.[19] The dissociation dynamics favor vibrationally cold and rotationally hot molecular nitrogen. The N_2 rotational distribution is peaked at $J = 74$,[19b] confirming the ab initio and vibronic structure analysis that the geometry of the upper state favors a bent molecule.

In 1993 Kim and Craig proposed that the N_2O isotopomer concentrations in the troposphere arise from a combination of light N_2O produced by soil, N_2O from the oceans, and a back flux of isotopically heavy N_2O from the stratosphere.[20] Photochemistry (reactions [1] and [2]) was identified as the source of the stratospheric enrichment. However, a study of the photolysis of N_2O at 185 nm indicated no significant enrichment,[16,21] and it was proposed that the accepted stratospheric chemistry be modified to incorporate new N_2O formation reactions involving radicals and/or molecules in excited states and molecular nitrogen.[22] Mass-independent enrichment in the three-isotope plot of atmospheric samples was taken to support the additional reactions.[23] At about the same time, Rahn and Wahlen showed that stratospheric air was enriched in ^{15}N and ^{18}O relative to tropospheric air in a pattern consistent with the standard photochemical sinks.[24]

The state of knowledge was improved considerably by Yung and Miller's zero point energy (ZPE) model, which provides a wavelength-dependent explanation for isotopic enrichment through the stratospheric photolysis of N_2O.[25] The natural abundances of N and O isotopes are shown in Table 1 along with the abundances of the N_2O isotopomers. For simplicity, the isotopomer $^{14}N^{14}N^{16}O$ will be written as 446, $^{14}N^{14}N^{18}O$ as 448, and so on. Yung and Miller observed that an isotopically substituted molecule will have a smaller ZPE than 446 and proposed that this results in a greater separation from the upper state and a blue-shifted spectrum (cf. Table 2). Since photolysis in the stratosphere takes place on the red shoulder of the peak, heavy isotopomers will have a lower cross-section, leading to their enrichment in the remaining sample. The model assumes that the potential energy surfaces are not affected by the mass of the nuclei. Further, the upper state is assumed to be repulsive, so that isotopic substitution shifts the energy levels on the lower bound surface but not the continuum levels of the upper surface. The ZPE model was able to explain the observed distribution of N_2O isotopomers without the new source reactions. The more general theory of photoinduced isotopic fractionation (PHIFE) has been extended in recent work and promises to be an important tool for investigating planetary atmospheres.[26]

TABLE 1: Natural Abundance (i.e., No Enrichment) of the Six Most Abundant N_2O Isotopomers[40] [a]

isotope	abundance/%	isotopomer	abundance/%
^{14}N	99.634	446	99.033
^{15}N	0.366	447	0.038
		448	0.198
^{16}O	99.762	456	0.364
^{17}O	0.038	546	0.364
^{18}O	0.200	556	0.001
		sum (446, 447, 448, 456, 546, 556):	99.998

[a] $^{14}N^{14}N^{16}O$ is abbreviated 446, and so on.

TABLE 2: Band Centers of the Fundamental Vibrational Frequencies of N_2O, Together with the Zero Point Energy (ZPE), and the Difference of the ZPE from the ZPE of the 446 Isotopomer (ΔZPE)[a]

ijk	ν_1	ν_2	ν_3	ZPE	ΔZPE
446	1284.903[b]	588.768[c]	2223.757[d]	2343.10	0.00
447	1264.704[b]	586.362[e]	2220.074[d]	2328.75	14.35
448	1246.885[b]	584.225[e]	2216.711[d]	2316.02	27.08
456	1280.354[b]	575.434[c]	2177.657[d]	2304.44	38.66
546	1269.892[b]	585.312[c]	2201.605[d]	2321.06	22.04
556	1265.334[b]	571.894[e]	2154.726[d]	2281.92	61.17

[a] Frequencies and energies are given in units of cm^{-1}. [b] Reference 41. [c] Reference 42. [d] Reference 43. [e] Reference 44.

Enrichment factors obtained from subsequent experiments were in qualitative agreement with the ZPE model but a factor of 2 higher than predicted (cf. Figure 5). Questions were raised about the role played by the transition dipole surface, upper-state dynamics and bending excitation, which are not included in the ZPE model. The goal of this article is to dissect the UV spectrum of N_2O and determine the contribution of the additional factors. The structure of the paper is as follows. The relative photolysis cross-sections of the most important isotopomers are calculated using a Hermite time propagation operator[27] and potential energy surfaces from the literature[18] and our own work. The isotopomer-specific UV absorption spectra contain contributions from the three lowest-bending vibrational states. The wavelength- and temperature-dependent isotopic enrichment factors calculated by the model are compared to laboratory experiments, stratospheric remote-sensing data, and the ZPE model. The results of the present model are found to be in good agreement with laboratory experiments and the stratospheric observations.

Theory

For the NN + O system we assume the following model Hamiltonian:[28]

$$H = -\frac{\hbar^2}{2\mu}\frac{\partial^2}{\partial R^2} - \frac{\hbar^2}{2}\left(\frac{1}{\mu R^2} + \frac{1}{m r_e^2}\right)\left(\frac{1}{\sin\theta}\frac{\partial}{\partial\theta}\sin\theta\frac{\partial}{\partial\theta}\right) + V(R,\theta) \quad (1)$$

where R is the distance from the oxygen atom to the center of mass of the nitrogen molecule and θ is the angle between the

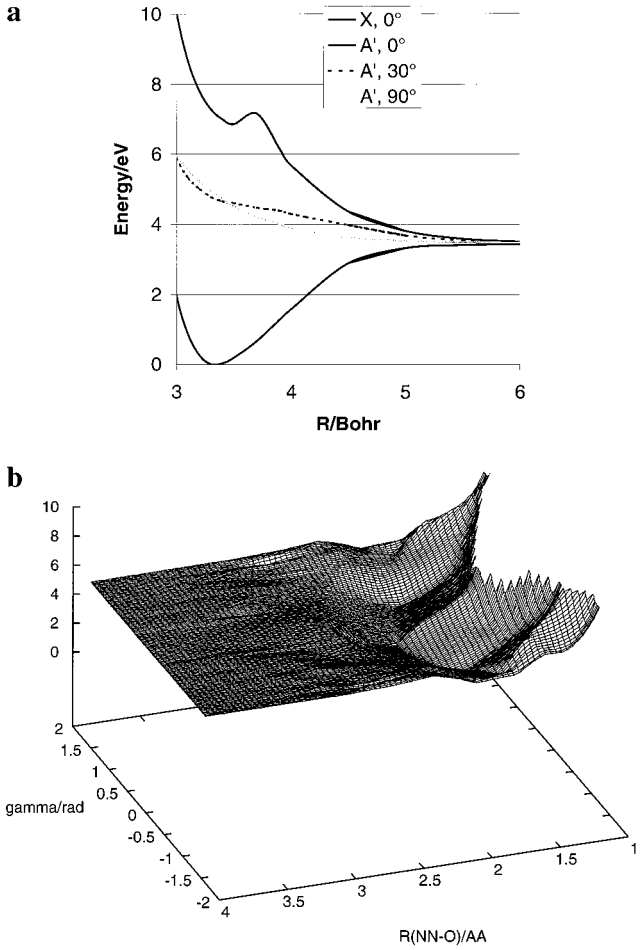

Figure 1. (a) Cuts through the ground $X1^1A'(^1\Sigma^+)$ and excited $2^1A'$-($^1\Delta$) potential energy surfaces are shown.[18] A vertical transition from the minimum of the ground-state surface leads to a location where the maximum gradient of the A′ surface is in the bending dimension instead of the bond-breaking dimension. (b) The excited-state potential energy surface (the units of the *Z*-axis are 100 kJ/mol).

NN and the *R* axis. The reduced masses μ and m are defined as

$$\mu = \frac{m_3(m_1 + m_2)}{m_1 + m_2 + m_3} \tag{2}$$

$$m = \frac{m_1 m_2}{m_1 + m_2} \tag{3}$$

where the masses are numbered from left to right in the NNO molecule. The interatomic N−N distance r_e is kept fixed in the calculations. The potential $V(R,\theta)$ is that of the upper electronic state. To calculate the absorption spectra, we use the relation[29]

$$\sigma(\omega) = C\omega \int_{-\infty}^{\infty} \mathrm{d}t \exp(iEt/\hbar)\left\langle \phi_0 \middle| \exp\left(-\frac{i}{\hbar} Ht\right) \middle| \phi_0 \right\rangle \tag{4}$$

where ϕ_0 is the initial wave function. The absorption spectrum is obtained as a Fourier transform with respect to the total energy $\{E = \hbar\omega + E_i$, where $E_i = \hbar\omega_1(n_1 + {}^1/_2) + 2\hbar\omega_2(n_2 + {}^1/_2) + \hbar\omega_3(n_3 + {}^1/_2)\}$ of the correlation function $\langle\phi(t_0)|\phi(t)\rangle$. Here $\phi(t_0) = \phi_0$, and $\phi(t)$ is the time-propagated wave function:

$$\phi(t) = \exp\left(-\frac{i}{\hbar} Ht\right)\phi(t_0) \tag{5}$$

To propagate the wave function, we use the so-called Hermite propagator,[27] which is based on the expression:

$$\exp(-iHt/\hbar) = \sum_{m=0}^{\infty} \frac{(-i)^m}{m!} r^m \exp(-\tau^2) H_m(H/\mathrm{E}_{\max}) \tag{6}$$

where $\tau = E_{\max}t/2\hbar$ and H_m is a Hermite polynomial. The Hermite propagator (HP) method improves on the well-known Chebyshev propagator, and is a computationally and numerically efficient formulation of the spectral filter problem, resulting in

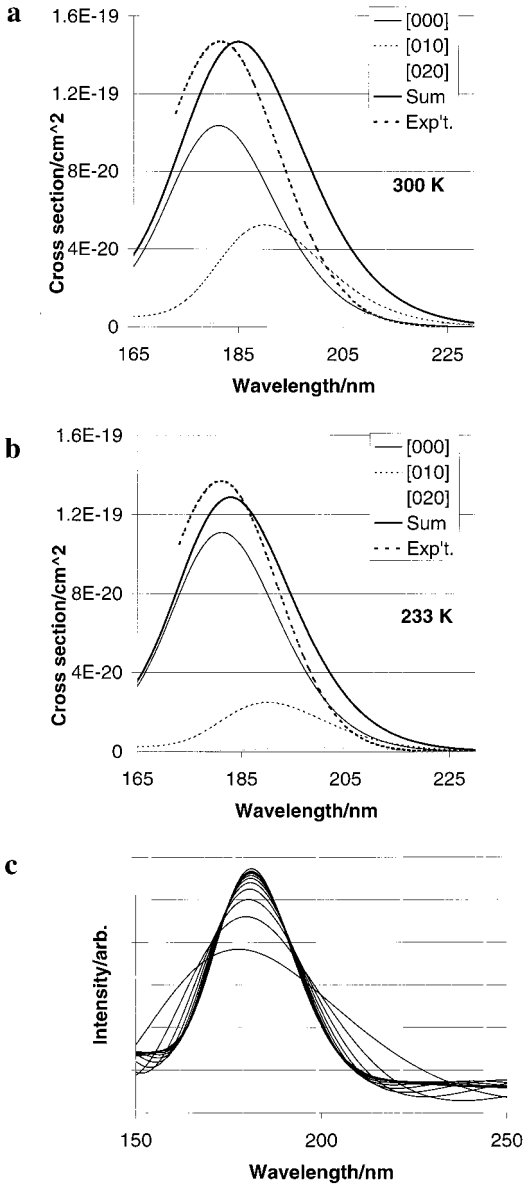

Figure 2. (a) A comparison of the calculated absorption spectrum for 446 N_2O at 300 K with the experimental absorption band.[6,13a] The calculated absorption is shifted to the red by ca. 1.5% in energy (or <3 nm) relative to experiment. The 446 spectrum contains contributions from the $n_2 = 0$, 1, and 2 vibrational states as shown (labeled 000, 010, and 020, respectively). The cross-sections shown for these states reflect the partition function at 300 K and the degeneracy of the bending states. (b) The same, but at 233 K, a temperature typical for the photolysis of N_2O in the stratosphere. (c) The enrichment is a sensitive function of the absorption cross-section. To ensure that the calculation was converged, a 40 000-term Hermite expansion was used. Starting with the widest function, the curves show the state of the correlation function for 1, 2, 3, 4, 5, 6, 7, 8, 9, 10, 20, 30, and 40 thousand terms. The last three overlap on this figure. Extension of the polynomial to 80 000 terms showed no significant difference from the result at 40 000 terms.

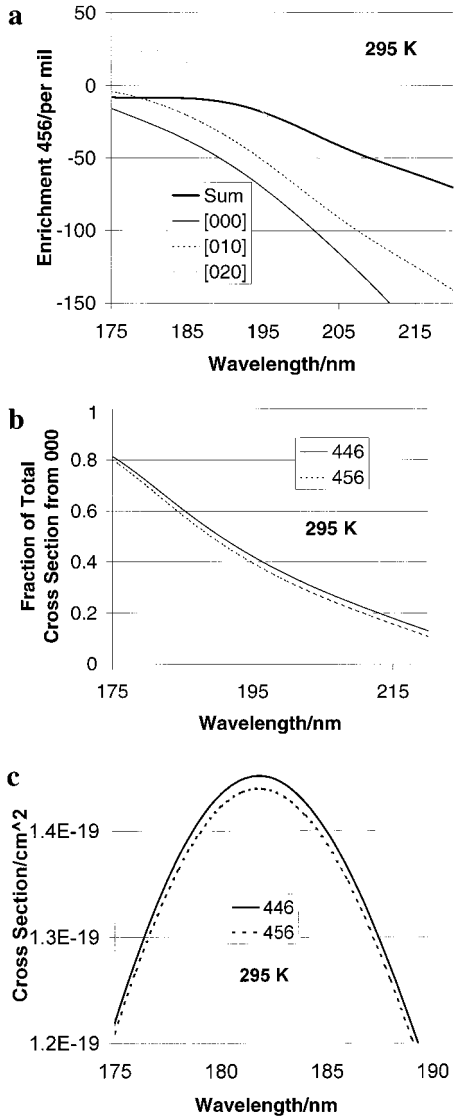

Figure 3. (a) The components of the enrichment of 456 N_2O are displayed. The bending ground state alone shows more enrichment than the excited bending states, and the total enrichment is less than would be apparent only from the consideration of the vibrational ground state. (b) The fraction of the absorption coming from the ground vibrational state is shown as a function of wavelength for the 446 and 456 isotopomers. (c) The HP model predicts that the enrichment arises from a shift in the intensity of the entire isotopomer band, in addition to a slight wavelength shift. The cross-section of the 446 and 456 isotopomers is compared at 295 K.

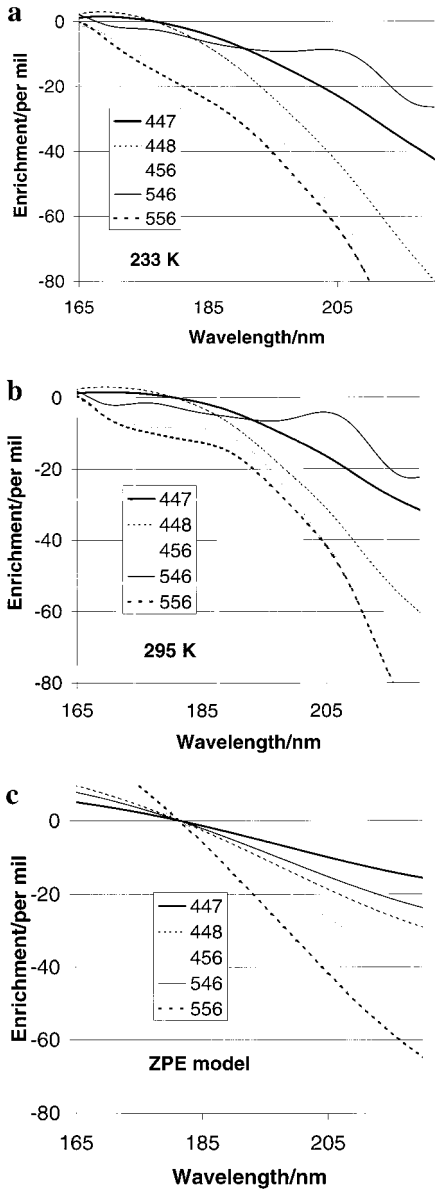

Figure 4. (a) The enrichment (defined in the text) of the most common N_2O isotopomers plotted vs wavelength, using the isotopomer cross-sections at 233 K. (b) 295 K. It is seen that the absolute value of the enrichment decreases with increasing temperature as explained in the text. (c) The results of the ZPE model, which are independent of temperature. The ZPE model predicts positive enrichments at wavelengths shorter than 182 nm, whereas the HP model predicts zero or slightly negative enrichments.

an exponentially convergent propagation scheme. E_{max} is a scaling energy, which for convenience is set to be the largest energy of the system. The wave function is propagated from $t_0 = 0$. The relation $\langle\phi_0|\phi(-t)\rangle = \langle\phi_0|\phi(t)^*\rangle$ is used for negative values of t. The time integral from $-\infty$ to $+\infty$ can then be performed analytically, leading to

$$\sigma(\omega) = \sum_{m=0}^{\infty} F_m(\omega) < \phi_0 | \frac{1}{\sqrt{2^m m!}} H_m(H/E_{max}) | \phi_0 > \quad (7)$$

where

$$F_m(\omega) = C\frac{\hbar\omega}{E_{max}} 2\sqrt{\pi}\exp(-y^2)\frac{H_m(y)}{\sqrt{m!2^m}} \quad (8)$$

and $y = E/E_{max}$. The summation is carried out using the recursion formula for Hermite polynomials, $H_m(x) = 2xH_{m-1} - 2(m-1)H_{m-2}$. A Morse wave function in the N−O bond (r') times a harmonic oscillator function in the bending angle γ was used to calculate the initial wave function on the ground electronic state. A simple "local mode" approach for the vibrational wave function was chosen so that the effect of isotopic substitution would be direct and independent of the model. Thus we have

$$\phi_0(r',\gamma) = \phi_m(r')\phi_H(\gamma) \quad (9)$$

where for the bending ground state

$$\psi_H(\gamma) = (2\beta_h/a)^{0.25}\exp\left(-\frac{1}{2}b_h\gamma^2/a\right) \quad (10)$$

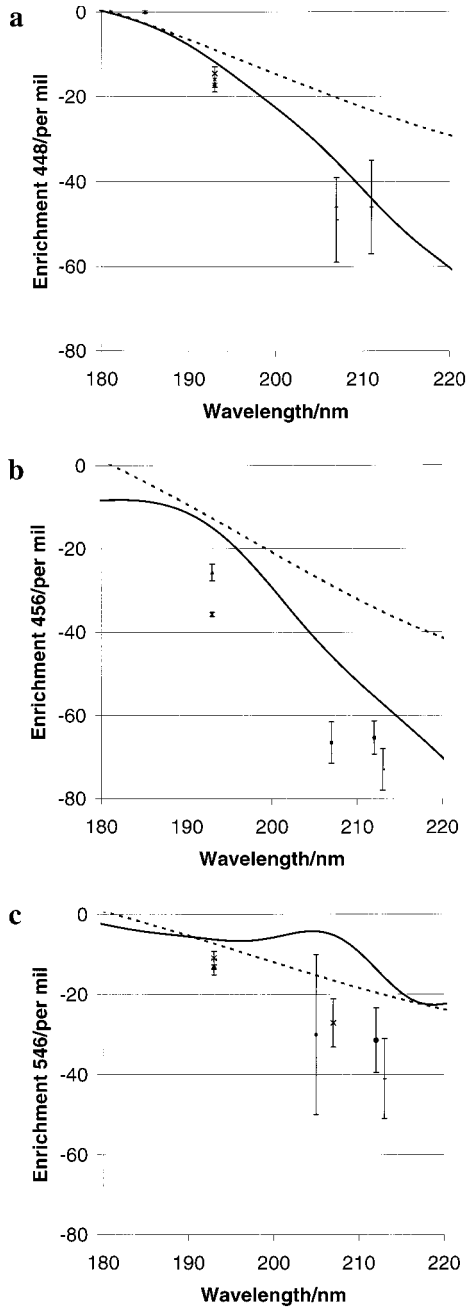

Figure 5. (a) A comparison of the calculated enrichment (solid line) with experiment and with the zero point energy model (dashed line) for 448 N_2O, 295 K. Experimental data is shown at the following wavelengths: 185 nm,[21] 193 nm (upper),[45] 193 nm (middle),[46] 193 nm (lower),[47] 207.6 nm (upper),[45] 207.6 nm (lower),[46] and 211.5 nm.[46] (b) Comparison for 456 N_2O, 295 K. Experimental data is shown at the following wavelengths: 193 nm (upper),[46] 193 nm (lower),[47] 207.6 nm,[46] 211.5 nm,[46] and 212.8 nm.[48] (c) Comparison for 546 N_2O, 295 K. Experimental data is shown at the following wavelengths: 193 nm (upper),[47] 193 nm (lower),[46] 205.5 nm,[34] 207.6 nm,[46] 211.5 nm,[46] and 212.8.[48] The uncertainty in the HP enrichment factors is estimated to be ca. 10 per mil.

Here β_h and a are defined as

$$\beta_h = \omega_h/\hbar \tag{11}$$

$$a = ((r_e + r_e')^2/m_2 + (r_e)^2/m_3 + (r_e')^2/m_1)/(r_e r_e')^2 \tag{12}$$

$$\omega_h = k\gamma r_e r_e' \sqrt{a} \tag{13}$$

TABLE 3: Intensity Factors $f_{ijk,m}$ of the Isotopomers in the Ground, First, and Second Bending Vibrational States[a]

isotopomer *ijk*	$f_{ijk,0}$	$f_{ijk,1}$	$f_{ijk,2}$
446	0.013574	0.034648	0.063470
447	0.013516	0.034464	0.063151
448	0.013465	0.034300	0.062865
456	0.013309	0.033722	0.061784
546	0.013513	0.034392	0.063010
556	0.013250	0.033475	0.061334

[a] The factor accounts for the product of the isotopomer-dependent vibrational wave function with the transition dipole surface.

The Morse parameters were obtained from the ground-state potential energy surfaces and the bending force constant taken as 0.49×10^5 dyn/cm.[30] To initialize the values of R and θ for the wave function, we used the following relations connecting the coordinates and angles:

$$r' = \sqrt{R^2 + (\epsilon r_e)^2 - 2\epsilon r_e R \cos\theta} \tag{14}$$

where $\epsilon = m_1/(m_1 + m_2)$. The calculation was carried out using

$$\gamma = \cos^{-1}((\epsilon r_e - R\cos\theta)/r_e') \tag{15}$$

a 128×128 grid with R in the range of 1−6 Å and θ between $-\pi/2$ and $+\pi/2$. Mass enters the calculation of the cross-section through the following terms: the reduced mass of the Morse oscillator for the N−O bond, the ZPE of the N_2O molecule E_i, the parameter a in the bending wave function, and the reduced mass of the relative motion μ and of the N_2 molecule m. In addition, the mass-dependent bending vibrational frequency changes the partition function and Boltzmann factors used to weigh the contribution from the various vibrational states. As shown below, the net effect is "mass-independent" fractionation, as defined by the mass spectroscopy community.

The absorption cross-section was calculated for the isotopomers 446, 447, 448, 456, 546, and 556. As seen in eq 16 below, $\sigma_{ijk}(T)$ depends on the result of the model calculation $\sigma_{ijk,m}$, the factor g_m representing the number of (pseudo)-degenerate angular momentum states of the degenerate bending mode ($g_m = m + 1$; e.g., for $m = 2$, there are three components, $02^{\pm 2}0$ and 02^00), an intensity factor representing the square of the integral of the vibrational wave function and transition dipole moment surface ($f_{ijk,m}$), the Boltzmann population factor, the partition function, and an arbitrary scaling factor C. The nuclei are represented by the labels i, j, and k. The ground, first, and second excited bending vibrational states were considered; values of $n_2 > 2$ are not important at the temperatures being considered because of the Boltzmann factor. To sum:

$$\sigma_{ijk}(T) = \frac{C\sum_{ijk,m}\sigma_{ijk,m}g_m f_{ijk,m}\exp\left(\dfrac{-m\nu_{ijk}^{\text{bend}}}{kT}\right)}{1 + 2\exp\left(\dfrac{-\nu_{ijk}^{\text{bend}}}{kT}\right) + 3\exp\left(\dfrac{-2\nu_{ijk}^{\text{bend}}}{kT}\right)} \tag{16}$$

The intensity factors $f_{ijk,m}$ are presented in Table 3.

A calculation of the potential energy surface of N_2O in the ground state was performed using Gaussian 98.[31] The potential minimum was found using the Moeler−Plesset MP2 method in the 6-311++G(3df,3pd) basis set.[32] The potential energy surface was created using a grid of geometries. The NN distance was fixed to the equilibrium value of 1.154388 Å, and the N−O distance varied from 0.96 to 11.17 Å. The result of our

calculation of the ground-state potential energy surface is not significantly different from that of Balint-Kurti and co-workers[18] but is useful because a larger range of geometries is explored.

Results and Discussion

1. The Temperature-Dependent UV Cross-Section. Figure 1a shows cuts through the $X1^1A'(^1\Sigma^+)$ and $2^1A'(^1\Delta)$ potential energy surfaces, and Figure 1b shows the $2^1A'$ surface itself. The ground state is at a minimum for the linear molecule, and the excited-state surface slopes downward as the molecule bends. Combined with a small barrier to direct dissociation for the linear species, this leads to a large rotational excitation of the N_2 photofragment. State-resolved product imaging experiments show 1.4 eV of rotational excitation, an amount of energy roughly equal to the translational energy of the photofragments.[19,33] Several workers have noted the importance of the bending vibration in the temperature dependence of the spectrum.[13,16,19b] Clearly, bending in the ground state will lead to a more favorable Franck−Condon factor with the upper state. In addition, the transition is orbitally forbidden for a linear molecule and vibronically allowed for the bent system. The transition dipole surface of Balint-Kurti and co-workers[18] displays a minimum for the linear system and increases with increasing bending angle. The maximum of the absorption curve, 182 nm, corresponds to an energy of 6.8 eV, which is not large enough to reach the minimum of the potential for a vertical transition to the linear excited state.

The results of the calculation for the main isotopomer are shown at 300 K (Figure 2a) and 233 K (Figure 2b). 446 NNO accounts for 99% of the molecules in a sample at natural abundance (Table 1), and so is representative of the UV absorption spectrum of the compound. The calculated relative cross-sections were scaled by a factor of 1.7×10^{-18} to match the experimental cross-section, also shown in Figure 2. The width of the absorption curve matches the experimental observation very well. There is a small shift in energy of about 1.5% (or 3 nm), perhaps due to remaining uncertainties in the calculation of the potential energy surfaces.

The absorption spectrum is composed of contributions from the ground, first, and second bending vibration states, with a higher "hot band" contribution at higher temperatures. These absorptions appear on the red shoulder of the curve, in the region of the stratospheric UV window. At room temperature, the fraction of molecules in the first excited bending mode is 10% (including degeneracy); even so, this accounts for a majority of the transition intensity at wavelengths longer than 200 nm. The model results indicate that the perpendicular $1^1A'' \leftarrow X^1A'$ transition does not make a significant contribution to the observed spectrum. The small transition dipole moment[18] leads to an intensity ca. 2.5% of that of the $2^1A' \leftarrow X^1A'$ transition, in agreement with the results of Janssen and co-workers.[17] Considering the transition dipole surface (and ignoring the Boltzmann factor), the transitions from the $n_2 = 0$, 1, and 2 states have an intensity ratio of ca. 1:3:6. Compared to experimental data, Figure 2b shows that the model results have a temperature dependence that is slightly too large, implying that the model may overestimate the contribution of the excited bending states. This may be due to the transition dipole surface, or the approximation used in obtaining the vibrational wave functions.

To demonstrate convergence, the results of the calculation for 446 in the $n_2 = 0$ vibrational state is shown in Figure 2c. For a 40 000-term Hermite expansion (cf. eq 7), the calculation was converged. Continuing the calculation to 80 000 terms did not significantly change the result.

2. Enrichment Factors. It is interesting to consider the lifetime of the dissociating system. The ZPE model assumes a repulsive excited state and direct dissociation; the isotope effect arises from the effect of mass on the ground-state energy levels. At the other extreme, as noted by Umemoto,[34] large isotope effects have been described for several predissociative systems.[35] As the lifetime of the excited-state wave function increases, we can expect the effect of isotopic substitution on the wave function on the upper state to play a larger role in determining the final enrichment. N_2O seems to be an intermediate case. Some fine structure is observed on the blue side of the absorption curve, corresponding to a bond angle of 115°, ν_1 of 1372 cm^{-1}, and ν_2 of 1761 cm^{-1}.[16] A Franck−Condon model[36] indicates that isotopic substitution has a significant effect on the wave function on the upper state, and thus the enrichment, and prompted us to initiate the present work to consider the effects in greater detail. A separate dynamics calculation indicates that after 1 ps, only 6% of the wave packet has left the potential energy grid of the calculation.[36] The long lifetime of the wave packet explains the structured absorption at wavelengths shorter than 180 nm.[13,16] (The experimental absorption cross-section shown in Figures 2a and 2b is based on a polynomial expression and does not have enough terms to show the fine structure). For a vertical transition from the minimum on the ground-state surface, the maximum gradient in the upper state corresponds to bending.

The origin of the enrichment is illustrated in Figure 3 for the 456 isotopomer. Enrichment is defined as $\epsilon = \alpha - 1$, where α is the ratio of the isotopomer to the reference reaction or photolysis rate, in this case $\alpha = \sigma_{456}/\sigma_{446}$. Because it is independent of the extent of reaction, the enrichment is a characteristic property of a given process. We have displayed ϵ for each of the vibrational states, and it is seen that the enrichment is largest for $n_2 = 0$ and smallest for $n_2 = 2$. A consideration of the vibrational energy of the systems involved using the ZPE model would predict the opposite trend, so the effect must arise from the upper state. A curious feature is that the total enrichment is less than would be predicted from simply considering the enrichment due to each vibrational component. Heavy systems have relatively greater populations in the $n_2 = 1$ and $n_2 = 2$ states (Figure 3b), and as shown in Figure 2 and Table 3, these states have disproportionately large cross-sections. Since the enrichment arises because heavy isotopomers have a relatively smaller absorption cross-section on the red shoulder of the absorption, this effect decreases the observed enrichment. It follows that greater absolute enrichments will be observed at lower temperatures; for example, our model predicts greater enrichments in stratospheric samples than for room-temperature photolysis experiments. Figure 3c shows that the enrichment arises largely from a shift in the intensity (cf. Table 3) of the absorption, in contrast to the ZPE model, in which the enrichment arises from a wavelength shift of the spectrum.

The enrichments of the most common isotopomers are shown at 233 and 295 K, respectively, in Figures 4a and 4b. 233 K was chosen because it is characteristic of the temperature of the stratosphere, where maximum photolysis occurs.[6,7] 295 K was chosen to represent the temperature of the laboratories in which photolysis experiments were conducted. Figure 4c shows the enrichments predicted by the ZPE model. This model does not consider excited bending vibrational states and is independent of temperature. The Hermite polynomial (HP) and ZPE models make the same general predictions regarding the ordering of isotopomer enrichments.

3. Comparison to Experimental and Stratospheric Enrichment Data. Figure 5a compares the results of several experiments, the ZPE model, and our model for the 448 isotopomer. The enrichment curve was calculated at 295 K and shifted by 3 nm to reflect the shift between the calculated UV spectrum and the experimental (Figure 2). Figure 5b presents the results for 456, and 5c presents those for 546. The agreement for the 448 and 456 isotopomers is satisfactory, given the approximations in the HP model. The uncertainty in the enrichments derived from the HP model are ca. 10 per mil, due to remaining uncertainties in the potential energy and dipole moment surfaces, errors in the local mode vibrational wave function, and uncertainties in the calculation itself. Due to the propensity of the excited state to bend, it is possible that the stimulated/resonant Raman cross-section for vibrational bending excitation in pulsed laser photolysis experiments may be high enough to transfer population into the excited bending modes and bias the results. A bump of ca. 5 enrichment units is apparent at 207 nm on the results of the HP model for the 546 isotopomer (see Figure 5c). This is due to a transition from a region where $n_2 = 1$ enrichment dominates to one where $n_2 = 0$ dominates. Closer inspection reveals this modulation in the enrichment plots of all the isotopomers (cf. Figures 4a and 4b).

Figures 6a to 6c show a comparison of the models with enrichment factors derived from data concerning the altitude profiles of N_2O isotopomers in the stratosphere.[49] The profiles were calculated based on infrared spectra measured using a balloon-based interferometer and used to derive enrichment factors for stratospheric photolysis. The HP model predicts larger absolute enrichment factors at low stratospheric temperatures due to the decreased population of the excited bending modes.

The radiative transfer model of Minschwaner, Salawitch, and McElroy indicates that the maximum photolysis rate for N_2O occurs at 200 nm and an altitude of 29 km, for equinox at 5° latitude, local noon.[7] The diurnal average photolysis rate has a maximum in the region of 0−15° latitude and at an altitude of ca. 31 km. The authors state that the photolysis rate for N_2O is largest at wavelengths between 195 and 205 nm, over an altitude range of 25−35 km. Work by Minshwaner indicates that the maximum actinic flux at a solar zenith angle of 30° occurs at 205 nm.[6] Following Yung and Miller,[25] in Figure 6 we take the wavelength of 205 nm as characteristic for the photolysis of N_2O in the stratosphere. While the temperature of N_2O will vary depending on season, altitude, and latitude, we have assumed a temperature of 233 K to be representative of the low-latitude stratosphere at an altitude of 30 km. The results of Griffith et al. for the isotopic enrichment of stratospheric N_2O are presented in Figure 6[49] and compared to the ZPE model and our model. Because of the decreased temperature, the model predicts a higher enrichment than at room temperature. With the possible exception of the 546 isotopomer, the HP model is in excellent agreement with the available stratospheric data.

As noted by Minschwaner,[7] there are significant contributions to the photolysis rate of N_2O associated with holes in the Shuman−Runge spectrum of molecular oxygen, between 188 and 195 nm. Based on the ZPE model (cf. Figure 4c), Rahn et al. have proposed that the positive enrichments in this region may help to explain why stratospheric enrichments are less than the experimental.[45] The HP model provides another explanation for the discrepancy. Since the bending vibrational distribution of a sample is important for determining its enrichment, lower enrichments are expected for photolysis at stratospheric temperatures compared to ambient laboratory experiments. As noted,

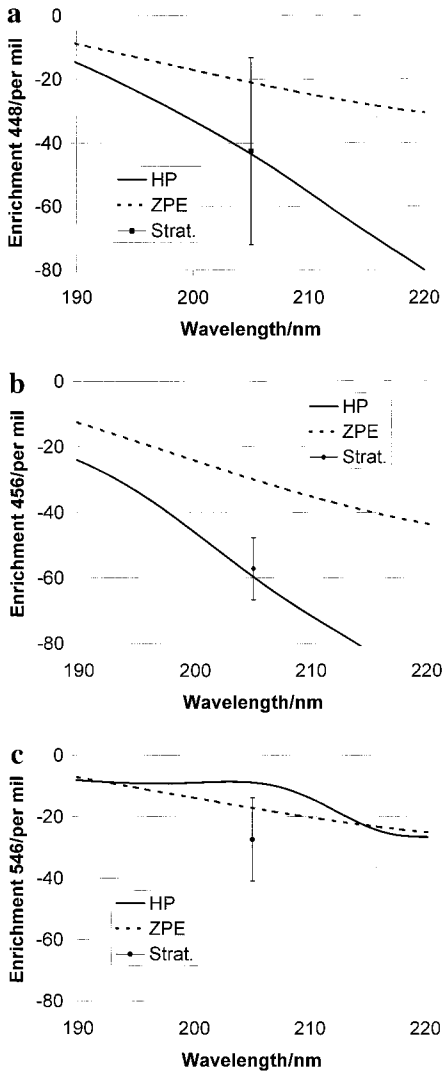

Figure 6. (a) Comparison with observed enrichment factors in the earth's stratosphere with model results for 233 K, 448 isotopomer. We take 205 nm as a representative wavelength for N_2O photolysis in the stratosphere. (b) The 456 isotopomer. (c) The 546 isotopomer. Stratospheric data from Griffith et al.[49]

the HP model predicts moderately to strongly negative enrichments at all wavelengths.

There is excess ^{17}O in atmospheric N_2O, relative to the isotope's nominal concentration in the environment, and further, the ^{17}O is enriched in a mass-independent manner.[37] A mass-dependent enrichment arises from processes such as diffusion and evaporation, whose rate depends on the mass of the molecule. The composition of a given sample is defined by the value $\delta = R_i/R_{std} - 1$, where R is the ratio of the concentration of the isotopically labeled species (e.g., 456) to the reference species (e.g., 446) for the isotopically enriched sample i and the reference standard. For a sink process with an isotopic signature ϵ, the composition can be approximated as $\delta_f = \delta_0 + \epsilon \ln(f)$, where f is the fraction of the original material remaining. For $\delta_0 = 0$, $\delta_f = \epsilon \ln(f)$. The traditional theory states that if we consider the three-isotope factor $\rho = {}^{17}\delta/{}^{18}\delta$ in N_2O, $\rho = 0.51$ for a mass-dependent process. Work by Thiemens et al. has indicated that $\rho > 0.51$ for stratospheric N_2O; i.e., there is excess ^{17}O.[37] Figure 7 shows the results of the model; "mass-independent" enrichment is predicted through photolysis in the stratosphere. Moreover the enrichment grows as temperature is decreased from ambient to stratospheric. The straight-dashed

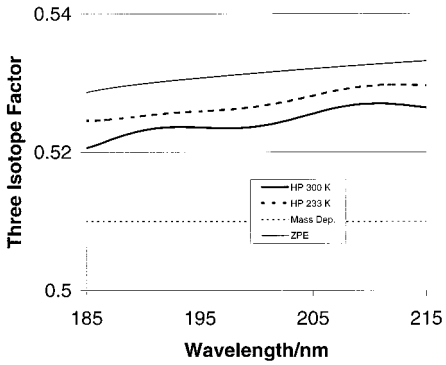

Figure 7. The cross sections of the three-isotope system 446, 447, and 448 indicate that "mass-independent" enrichment, as defined by the mass spectroscopy community, is predicted for photolysis throughout the range of wavelengths shown in the figure. The mass-dependent line is given by 0.51, as explained in the text. The figure displays the three-isotope factor for the HP model at 295 K, the HP model at 233 K, and the ZPE model.

line is characteristic of a mass-dependent enrichment. The three-isotope factor predicted by the ZPE model is shown for comparison. Both of these models indicate that the UV photolysis of N_2O is not a "mass-dependent" process.

Conclusion

This paper has considered the behavior of the UV spectrum of N_2O on the red shoulder of the absorption peak, in the region where absorption by the bending hot bands is important. It is interesting to compare the transition intensity factors $f_{ijk,m}$ for the various isotopomers, as shown in Table 3. A decrease in intensity factor with decreasing ZPE (isotopic substitution) is observed. This can be understood as follows. The amplitude of the bending motion is greater for a light isotopomer. Since for N_2O the transition dipole moment and absorption cross-section are a sensitive function of bending angle, this results in an intensity change at all excitation wavelengths. In contrast, in the ZPE model the area under the absorption curve is constant for each isotopomer; only the position of the curve is changed. Thus the ZPE model predicts positive enrichments on the blue side of the peak, whereas the HP model predicts enrichments that are near zero or slightly negative. An experimental determination of the enrichment factors for N_2O at wavelengths between 165 and 185 nm would be useful, given a suitable light source. Another approach is to choose a system where readily available photolysis sources lie on the blue side of the absorption maximum. We have begun such studies on the molecule carbonyl sulfide and will report the results of our experiments and a comparison to the HP and ZPE models in a future publication.[8] It is interesting to note that experiments are underway on the vibrational state-selected photodissociation of N_2O isotopomers.[17c]

The HP model can correctly account for the observed distribution of 456, 546, and 448 isotopomers. The results of this calculation indicate that the standard model for the chemistry of the stratosphere[6] is complete without additional N_2O source mechanisms. In addition, recent experimental studies have cast doubt on the mechanisms.[38]

Toyoda and co-workers have recently demonstrated that ^{15}N and ^{18}O are enriched by about twice as much in the high stratosphere ($z > 24.1$ km) compared to the low stratosphere ($z < 24.1$ km).[39] This would initially appear to contradict our conclusion that smaller absolute enrichments are expected at higher temperatures, since temperature increases with altitude in the stratosphere. However, Figures 4a and 4b show that photolysis wavelength has a larger effect on isotopic enrichment than temperature. With increasing altitude, one passes through the Chapman layer, and long-wavelength absorption by O_3 decreases more rapidly than short-wavelength absorption by O_2.[6,7] Thus, at higher altitudes there is expected to be more photolysis at longer wavelengths where stronger enrichment factors pertain.

The HP method has allowed an examination of the effect of isotopic substitution, bending vibrational excitation, and transition dipole moment surface on isotopic enrichment through the photolysis of N_2O. The computation of the cross-sections was run on a PC. However the method requires high-quality potential energy and dipole moment surfaces of the ground and excited states. In contrast, the ZPE method uses readily available spectroscopic data. Using the Hermite propagator method, we have sought to extend the utility of predictions made using the ZPE model. For systems such as N_2O, where the sloping transition dipole surface makes the absorption cross-section dependent on bending motion, low-lying vibrational states play an important role. Further, the lifetime of the system on the upper state indicates it is not purely dissociative. These factors lead the ZPE model to underestimate the enrichment factors for N_2O. However, this should not limit its use for estimating isotope effects in systems for which those constraints do not apply. In conclusion, we anticipate that a great deal of experimental and theoretical activity will continue to be associated with isotopic fractionation effects in planetary atmospheres. Miller and Yung's photoinduced isotopic fractionation (PHIFE) theory is independent of a specific model for the mechanism of the enrichment.[26]

Acknowledgment. We wish to thank the Danish Natural Sciences Research Council, the Nordic Network for Chemical Kinetics sponsored by the Nordic Academy for Advanced Study, and the Lund University Supercomputing Center. In addition, we wish to acknowledge valuable conversations and/or correspondence with Y. L. Yung, C. E. Miller, G. A. Blake, P. Wine, N. W. Larsen, G. C. Groenenboom and O. J. Nielsen. Blake, Wine, and Miller graciously shared material prior to publication.

References and Notes

(1) (a) Khalil, M. A. K.; Rasmussen, R. A. *Ann. Glac*. **1988**, *10*, 73. (b) Leuenberger, M.; Siegenthaler, U. *Nature* **1992**, *360*, 449. (c) Machida, T.; Nakazawa, T.; Jujii, Y.; Aoki, S.; Watanabe, O. *Geophys. Res. Lett.* **1995**, *22*, 2921.

(2) (a) Thiemens M. H.; Trogler, W. *Science* **1991**, *251*, 932. (b) Khalil, M. A. K.; Rasmussen, R. A. *J. Geophys. Res.* **1992**, *97*, 14651. (c) Nevison, C. D.; Holland, E. A. *J. Geophys. Res.* **1997**, *102*, 25519. (d) Becker, K. H.; Lørzer, J. C.; Kurtenbach, R.; Wiesen, P.; Jensen, T. E.; Wallington, T. J. *Environ. Sci. Technol.* **1999**, *33*, 4134. (e) *Summary for Policy Makers*, IPCC 2001.

(3) Yung, Y. L.; Wang, W. C.; Lacis, A. A. *Geophys. Res. Lett.* **1976**, *3*, 619.

(4) (a) Stevens, C. M.; Krout, L.; Walling, D.; Venters, A.; Engelkemeir, A.; Ross, L. E. *Earth Planet. Sci. Lett.* **1972**, *16*, 147. (b) Moore, H. *Tellus* **1973**, *26*, 169. (c) Mauersberger, K. *Geophys. Res. Lett.* **1987**, *14*, 80. (d) Wahlen, M.; Tanaka, N.; Henry, R.; Deck, B.; Zeglen, J.; Vogel, J. S.; Southon, J.; Shemesh, A.; Fairbanks, R.; Broecker, W. *Science* **1989**, *245*, 286. (e) Manning, M. R.; Brenninkmeijer, C. A. M.; Allan, W. *J. Geophys. Res.* **1997**, *102(D9)*, 10673. (f) Roeckmann, T.; Brenninkmeijer, C. A. M.; Saueressig, G.; Bergamaschi, P.; Crowley, J. N.; Fischer, H.; Crutzen, P. J. *Science* **1998,** *281*, 544. (g) Weston, R. E. *Chem. Rev.* **1999**, *99*, 2115. (h) Yoshida, N.; Toyoda, S. *Nature* **2000**, *405*, 330.

(5) See for example (a) Kim, K.-R.; Craig, H. *Nature* **1990**, *347*, 58. (b) Naqvi, S. W. A.; Yoshinari, T.; Jayakumar, D. A.; Altabet, M. A.; Narvekar, P. V.; Devol, A. H.; Brandes, J. A.; Codispoti, L. A. *Nature* **1998**, *394*, 463. (c) Mandernack, K. W.; Rahn, T.; Kinney, C.; Wahlen, M. *J. Geophys. Res.* **2000**, *105*, 17709. (d) *Atmospheric Nitrous Oxide*; Khalil, M. A. K., Ed.; *Chemosphere: Global Change Science*, **2000**, *2*, 233−500.

(6) De More, W. B.; Sander, S. P.; Howard, C. J.; Ravishankara, A. R.; Golden, D. M.; Kolb, C. E.; Hampson, R. F.; Kurylo, M. J.; Molina, M. J. *Chemical Kinetics and Photochemical Data for Use in Stratospheric Modeling, Evaluation Number 12*, JPL Publication 97-4, Jet Propulsion Laboratory, California Institute of Technology: Pasadena, 1997.

(7) Minschwaner, K.; Salawitch R. J.; McElroy, M. B. *J. Geophys. Res.* **1993**, *98(D6)*, 10543.

(8) Johnson, M. S.; Billing, G. D.; von Hessberg, P.; Lassen, B.; Nanbu, S. *J. Geophys. Res. Atmos.*, in press.

(9) Okabe, H. *Photochemistry of Small Molecules*; John Wiley and Sons: New York, 1978; Chapter 6.

(10) Cantrell, C. A.; Shetter R. E.; Calvert, J. G. *J. Geophys. Res.* **1994**, *99*, 3739.

(11) Fahey, D. W.; Solomon, S.; Kawa, S. R.; Loewenstein, M.; Podolske, J. R.; Strahan, S. E.; Chan, K. R. *Nature* **1990**, *345*, 698.

(12) (a) Crutzen, P. J. *Q. J. Royal Meteorol. Soc.* **1970**, *96*, 320. (b) Crutzen, P. J. *J. Geophys. Res.* **1971**, *76*, 7311. (c) Johnston, H. S. *Science* **1971**, *173*, 517.

(13) (a) Selwyn, G.; Podolske, J.; Johnston, H. S. *Geophys. Res. Lett.* **1977**, *4*, 427. (b) Hubrich, C.; Stuhl, F. *J. Photochem.* **1980**, *12*, 93. (c) Merienne, M. F.; Coquart, B.; Jenouvrier, A. *Planet. Space Sci.* **1990**, *38*, 617.

(14) Hopper, D. G. *J. Chem. Phys.* **1984**, *80*, 4290.

(15) Neyer, D. W.; Heck, A. J. R.; Chandler, D. W. *J. Chem. Phys.* **1999**, *110*, 3411.

(16) Selwyn, G. S.; Johnston, H. S. *J. Chem. Phys* **1981**, *74*, 3791.

(17) (a) Janssen, M. H. M. *Faraday Discuss.* **1997**, *108*, 435. (b) Janssen, M. H. M. *Faraday Discuss.* **1999**, *113*, 473. (c) Teule, J. M.; Groenenboom, G. C.; Neyer, D. W.; Chandler, D. W.; Janssen, M. H. M. *Chem. Phys. Lett.* **2000**, *320*, 177.

(18) Brown, A.; Jimeno, P.; Balint-Kurti, G. G. *J. Phys. Chem. A* **1999**, *103*, 11089.

(19) (a) Felder, P.; Haas B.-M.; Huber, J. R. *Chem. Phys. Lett.* **1991**, *186*, 177. (b) Hanisco, T. F.; Kummel, A. C. *J. Phys. Chem.* **1993**, *97*, 7242. (c) Springsteen, L. L.; Satyapal, S.; Matsumi, Y.; Dobeck, L. M.; Houston, P. L. *J. Phys. Chem.* **1993**, *97*, 7239. (d) Suzuki, T.; Katayanagi, H.; Mo Y.; Tonokura, K. *Chem. Phys. Lett.* **1996**, *256*, 90.

(20) Kim, K.-R.; Craig, H. *Science* **1993**, *262*, 1855.

(21) Johnston, J. C.; Cliff, S. S.; Thiemens, M. H. *J. Geophys. Res.* **1995**, *100(D8)*, 16801.

(22) (a) Prasad, S. S. *J. Geophys. Res.* **1994**, *99(D3)*, 5285 and references therein. (b) McElroy M. B.; Jones, D. B. A. *Glob. Biogeochem. Cycles* **1996**, *10*, 651. (c) Zipf, E. C.; Prasad, S. S. *Geophys. Res. Lett.* **1998**, *25*, 4333. (d) Zipf, E. C.; Prasad, S. S. *Science* **1998**, *279*, 211.

(23) Cliff, S. S.; Thiemens, M. H. *Science* **1997**, *278*, 1774.

(24) Rahn, T.; Wahlen, M. *Science* **1997**, *278*, 1776.

(25) Yung, Y. L.; Miller, C. E. *Science* **1997**, *278*, 1778.

(26) (a) Miller, C. E.; Yung, Y. L. *Chemosphere-Global Change Science* **2000**, *2*, 255. (b) Miller, C. E.; Yung, Y. L. *J. Geophys. Res.* **2000**, *105-(D23)*, 29039.

(27) Vijay, A.; Wyatt, R. E.; Billing, G. D. *J. Chem. Phys.* **1999**, *111*, 10794.

(28) Tennyson, J.; Sutcliffe, B. T. *J. Chem. Phys.* **1982**, *77*, 4061.

(29) (a) Heller, E. J. *J. Chem. Phys.* **1978,** *68*, 2066. (b) *Acc. Chem. Res.* **1981**, *14*, 368.

(30) Herzberg, G. *Molecular Spectra and Molecular Structure II. Infrared and Raman Spectra of Polyatomic Molecules*; Van Nostrand: New York, 1945.

(31) Frisch, M. J.; Trucks, G. W.; Schlegel, H. B.; Scuseria, G. E.; Robb, M. A.; Cheeseman, J. R.; Zakrzewski, V. G.; Montgomery, J. A., Jr.; Stratmann, R. E.; Burant, J. C.; Dapprich, S.; Millam, J. M.; Daniels, A. D.; Kudin, K. N.; Strain, M. C.; Farkas, O.; Tomasi, J.; Barone, V.; Cossi, M.; Cammi, R.; Mennucci, B.; Pomelli, C.; Adamo, C.; Clifford, S.; Ochterski, J.; Petersson, G. A.; Ayala, P. Y.; Cui, Q.; Morokuma, K.; Malick, D. K.; Rabuck, A. D.; Raghavachari, K.; Foresman, J. B.; Cioslowski, J.; Ortiz, J. V.; Stefanov, B. B.; Liu, G.; Liashenko, A.; Piskorz, P.; Komaromi, I.; Gomperts, R.; Martin, R. L.; Fox, D. J.; Keith, T.; Al-Laham, M. A.; Peng, C. Y.; Nanayakkara, A.; Gonzalez, C.; Challacombe, M.; Gill, P. M. W.; Johnson, B.; Chen, W.; Wong, M. W.; Andres, J. L.; Gonzalez, C.; Head-Gordon, M.; Replogle, E. S.; Pople, J. A. *Gaussian 98, Revision A.5*; Gaussian, Inc.: Pittsburgh, 1998.

(32) (a) Pople, J. A.; Head-Gordon, M.; Fox, D. J.; Raghavachari, K.; Curtiss, L. A. *J. Chem. Phys.* **1989**, *90*, 5622. (b) Curtiss, L. A.; Jones, C.; Trucks, G. W.; Raghavachari, K.; Pople, J. A. *J. Chem. Phys.* **1990**, *93*, 2537.

(33) Neyer, D. W.; Heck, A. J. R.; Chandler, D. W.; Teule, J. M.; Janssen, M. H. M. *J. Phys. Chem. A* **1999**, *103*, 10388.

(34) Umemoto, H. *Chem. Phys. Lett.* **1999**, *314*, 267.

(35) (a) van de Runstraat, C. A.; deHeer, F. J.; Govers, T. R. *Chem. Phys.* **1974**, *3*, 431. (b) Govers, T. R.; van de Runstraat C. A.; deHeer, F. J. *Chem. Phys.* **1975,** *9*, 285. (c) Roche, A. L.; Tellinghuisen, J. *Mol. Phys.* **1979**, *38*, 129. (d) Sur, A.; Nguyen, L.; Nikoi, N. *J. Chem. Phys.* **1992**, *96*, 6791.

(36) Billing, G. D.; Johnson, M. S. Unpublished results, 2001.

(37) (a) Cliff, S. S.; Thiemens, M. H. *Science* **1997**, *278*, 1774. (b) Cliff, S. S.; Brenninkmeijer, C. A. M.; Thiemens, M. H. *J. Geophys. Res.* **1999**, *104(D13)*, 16171.

(38) (a) Estupiñán, E. G.; Stickel, R. E.; Wine, P. H. *Chemosphere-Global Change Science* **2000**, *2*, 247. (b) Estupiñán, E. G.; Stickel, R. E.; Wine, P. H. *Chem. Phys. Lett.* **2001**, *336*, 109.

(39) Toyoda, S.; Yoshida, N.; Urabe, T.; Aoki, S.; Nakazawa, T.; Suguwara, S.; Honda, H. *J. Geophys. Res.* **2001**, *106*, 7515.

(40) Lide, D. R. *CRC Handbook of Chemistry and Physics*, 79th ed.; CRC Press: New York, 1998.

(41) Toth, R. A. *J. Opt. Soc. Am. B.* **1986**, *3*, 1263.

(42) Jolma, K.; Kauppinen, J.; Horneman, V.-M. *J. Mol. Spectrosc.* **1983**, *101*, 278.

(43) Toth, R. A. *J. Opt. Soc. Am. B.* **1987**, *4*, 357.

(44) Amiot, C. *J. Mol. Spectrosc.* **1976**, *59*, 380.

(45) Rahn, T.; Zhang, H.; Wahlen, M.; Blake, G. A. *Geophys. Res. Lett.* **1998**, *25*, 4489.

(46) Turatti, F.; Griffith, D. W. T.; Wilson, S. R.; Esler, M. B.; Rahn, T.; Zhang, H.; Blake, G. A. *Geophys. Res. Lett.* **2000**, *27*, 2489.

(47) Roeckmann, T.; Brenninkmeijer, C. A. M.; Wollenhaupt, M.; Crowley, J. N.; Crutzen, P. J. *Geophys. Res. Lett.* **2000**, *27*, 1399.

(48) Zhang, H.; Wennberg, P. O.; Wu, V. H.; Blake, G. A. *Geophys. Res. Lett.* **2000**, *27*, 2481.

(49) Griffith, D. W. T.; Toon, G. C.; Sen, B.; Blavier, J.-F.; Toth, R. A. *Geophys. Res. Lett.* **2000**, *27*, 2485.